# Quantum dressed classical mechanics: Application to chemical reactions

**ARTICLE** *in* CHEMICAL PHYSICS LETTERS · JULY 2001

Impact Factor: 1.9 · DOI: 10.1016/S0009-2614(01)00555-3



**2 AUTHORS**, INCLUDING:

Cecilia Coletti
Università degli Studi G. d'Annunzio C…

**56** PUBLICATIONS **721** CITATIONS

SEE PROFILE

6 July 2001

ELSEVIER

Chemical Physics Letters 342 (2001) 65–74

CHEMICAL PHYSICS LETTERS

www.elsevier.com/locate/cplett

# Quantum dressed classical mechanics: application to chemical reactions

Cecilia Coletti [a], Gert D. Billing [b,*]

[a] *Dipartimento di Chimica, Università di Perugia, I-06123 Perugia, Italy*

[b] *Department of Chemistry, H.C. Ørsted Institute, University of Copenhagen, DK-2100 Ø, Copenhagen, Denmark*

Received 2 March 2001; in final form 24 April 2001

**Abstract**

Reaction dynamics of a four atom system is investigated using a time-dependent Gauss-Hermite discrete variable representation (TDGH-DVR) method. The method is applied to the description of vibrational degrees of freedom in the calculation of initially state selected cross-sections for the reaction $H_2 + CN \rightarrow HCN + H$, while translational and rotational motions are treated classically. 

## 1. Introduction

The utilization of quantum-classical methods for the treatment of molecular dynamic problems, in particular for $N$-body systems (with $N > 3$), for which a full quantal approach is numerically cumbersome, is extremely attractive since it attempts to incorporate the most important quantum effects in a framework which maintains the classical simplicity – both conceptual and computational – connected to the integration of the equations of motion.

During the last years an approach has been formulated [1–5], which allows the rigorous derivation of a quantum-classical theory. This method is founded on Gauss-Hermite (G-H) functions [1,6] used as expansion basis set: the set is centered around the classical trajectory and expands around it as time propagates; with a sufficient number of functions the method converges to the exact quantum result.

From a computational point of view this approach is particularly advantageous if the possibility of constructing a time-dependent discrete variable representation (DVR) method based on the G-H functions [7–10] is exploited: the grid points are found as zeroes of the Hermite polynomials themselves and move according to the dynamics of the system. This formulation presents several benefits: it permits to build a localized grid: the points gather and move where it is needed (i.e., where the system dynamics evolves), so that relatively less points are necessary, thus reducing the computational load. Like for ordinary grid methods the potential energy matrix is diagonal, furthermore no evaluation of kinetic energy operators is necessary during each time-step: the coupling elements are time-independent; the coupling matrix is diagonally dominant and this feature makes the Lanczos method particularly suitable for time propagation. In addition a combined split-Lanczos method has been recently developed [11],

* Corresponding author. Fax.: +45-35-32-02-59.
*E-mail address:* gdb@theory.ki.ku.dk (G.D. Billing).

0009-2614/01/$ - see front matter 
PII: S0009-2614(01)00555-3

allowing a drastic reduction of the number of iterations needed for convergence, thus making the method extremely competitive as far as computational time is concerned.

The aim of this work is an exploration of the possibility to use this approach for the description of reaction dynamics in many body systems.

Here we will limit ourselves to apply it to just two degrees of freedom of a four atom system – the reaction $H_2 + CN \rightarrow HCN + H$ – while the remaining variables are treated classically, as we did in [12]. However, the difference between the theoretical foundations of the two treatments is sensible: while the method of [12] is a 'primitive approach' to mixed quantum-classical theories, based essentially upon the use of an Ehrenfest averaged effective potential, the time-dependent discrete variable representation employed here for the vibrations of the two diatoms, i.e., the quantal degrees of freedom, can be rigorously derived from first principles, as mentioned before.

It is worth noting that an important feature of mixed quantum-classical approaches is that no dynamical constraints (no fixed bond lengths or angle values) are introduced as is the case in most reduced dimensionality methods: the system is still treated in its full dimensionality, but the computational requirements are not very large, especially compared to those needed in exact quantal methods.

Initially state selected cross-sections for the vibrational ground states of the reagents have been calculated using the potential energy surface of [13]; the computation of cross-sections for excited vibrational states and thermal rate constants, although possible within this method, is not dealt within this work, which is focused on testing the time-dependent DVR method for the dynamics of many body systems. The following step will be a quantum treatment of all the degrees of freedom of the system within this framework. In this respect it may be mentioned that the method has already been used to treat up to six dimensions [14] using between 10 and 20 grid points in each mode. An accurate representation of the vibrational/rotational wave function can be obtained with about 20 grid points in each of the three Jacobi degrees of freedom $(x, y, z)$ specifying the orientation and bond length for a diatomic molecule [9,10,14].

## 2. Method

The Hamiltonian for a system of two diatoms in a space-fixed Jacobi coordinate frame, where, for the case investigated here, $\mathbf{r}_1$ and $\mathbf{r}_2$ are the bond distances for CN and $H_2$, respectively, and $\mathbf{r}_3$ is the vector connecting the centers of mass of the two molecules, can be written as [12,15]

$$\hat{H} = -\sum_{i=1}^{3} \frac{\hbar^2}{2\mu_i} \left[ \frac{\partial^2}{\partial r_i^2} + \frac{1}{r_i^2} \left( \frac{\partial^2}{\partial \theta_i^2} + \cot\theta_i \frac{\partial}{\partial \theta_i} + \frac{1}{\sin^2\theta_i} \frac{\partial^2}{\partial \phi_i^2} \right) \right] + V(r_i, \theta_i, \phi_i), \tag{1}$$

where the Jacobi vector $\mathbf{r}_i$ is expressed in terms of its spherical polar components $r_i$, $\theta_i$ and $\phi_i$; $\mu_1$ and $\mu_2$ are the reduced masses for the two diatoms and

$$\mu_3 = \frac{(m_C + m_N)(m_H + m_H)}{(m_C + m_N + m_H + m_H)}. \tag{2}$$

As in [12] we will treat quantum mechanically the vibrational degrees of freedom of the reactants, $r_1$ and $r_2$, and classically the remaining variables. Anyway for the quantum treatment, instead of the grid method employed in [12], use will be made of the time-dependent discrete variable approach described in [7–10].

In the time-dependent Gauss-Hermite discrete variable representation (TDGH-DVR) method the wave function $\Psi(r_1, r_2, t)$ is expanded in the G-H basis set [1]

$$\Psi(r_1, r_2, t) = \sum_{n_1, n_2} a_{n_1, n_2} \Phi_{n_1}(r_1, t) \Phi_{n_2}(r_2, t) \phi_{n_1}(r_1, t) \phi_{n_2}(r_2, t), \tag{3}$$

where

$$a_{n_1, n_2} = \sum_{i=1}^{N_1} \sum_{j=1}^{N_2} c_{ij}(t) \phi_{n_1}(z_i) \phi_{n_2}(z_j) \tag{4}$$

so that the DVR basis functions themselves are

$$\psi_{ij}(r_1,r_2,t)=\Phi_{n_1}(r_1,t)\Phi_{n_2}(r_2,t)\sum_{n_1=0}^{N_1-1}\sum_{n_2=0}^{N_2-1}\phi_{n_1}(\xi_1,t)\phi_{n_2}(\xi_2,t)\phi_{n_1}(z_i)\phi_{n_2}(z_j), \quad (5)$$

where $\Phi_{n_k}(r_k,t)$ is

$$\Phi_{n_k}(r_k,t)=\pi^{1/4}\exp\left(\frac{\mathrm{i}}{\hbar}(\gamma_k(t)+p_k(t)(r_k-r_k(t))\right)+\mathrm{Re}A_k(t)(r_k-r_k(t))^2) \quad (6)$$

with $k=1,2$ and

$$\phi_{n_k}(\xi_k,t)=\frac{1}{\sqrt{n_k!2^{n_k}\sqrt{\pi}}}H_{n_k}(\xi_k)\exp\left(-\frac{1}{2}\xi_k^2\right) \quad (7)$$

where $H_{n_k}(\xi_k)$ is an Hermite polynomium and

$$\xi_k=\sqrt{2\mathrm{Im}A_k(t)/\hbar}(r_k-r_k(t)). \quad (8)$$

Thus $r_k(t)$ is the center of the wave packet in $r_k$, which, in its ground state, i.e., when $n_k=0$, is a Gaussian wave packet. The basis set is also characterized by a momentum parameter $p_k(t)$, by a width parameter $A_k(t)$ and by a phase $\gamma_k(t)$.

$N_1$ and $N_2$ are the orders of Hermite polynomials used in $r_1$ and $r_2$, respectively, and thus they represent the number of grid points in each quantum degree of freedom. In this way the grid points in the $k$th degree of freedom are determined by the number of zeroes of the $N_k$th Hermite polynomium and their position is not fixed in time, but it varies as a function of the time-dependent variables $\mathrm{Im}A_k(t)$ and $r_k(t)$, being

$$r_{k,i}=r_k(t)+\sqrt{\frac{\hbar}{2\mathrm{Im}A_k(t)}}z_i, \quad k=1,2 \quad (9)$$

for the $i$th grid point, where $z_i$ is the $i$th zero of the Hermite polynomial of order $N_k$.

The G-H basis functions are orthonormalized

$$\int \mathrm{d}r_k\Phi_{n_k}(r_k,t)\phi_{n_k}(\xi_k,t)\Phi_{m_k}(r_k,t)\phi_{m_k}(\xi_k,t)=\delta_{n_k,m_k} \quad (10)$$

if the following relation is used for $\mathrm{Im}\gamma_k(t)$

$$\mathrm{Im}\gamma_k(t)=-\frac{\hbar}{4}\ln\left(\frac{2\mathrm{Im}A_k(t)}{\pi\hbar}\right) \quad (11)$$

while the DVR basis functions are orthorgonal

$$\int \mathrm{d}r_1\mathrm{d}r_2\psi_{ij}(r_1,r_2,t)\psi_{lm}(r_1,r_2,t)=\delta_{i,l}\delta_{j,m}\mathcal{N}_i^{(1)}\mathcal{N}_j^{(2)} \quad (12)$$

or, by using Eq. (10)

$$\sum_{n_k=0}^{N_k-1}\phi_{n_k}(z_i)\phi_{n_k}(z_j)=\delta_{i,j}\mathcal{N}_i^{(k)}. \quad (13)$$

If we insert the expansion (3) in the Schrödinger equation for the vibrations of the two diatoms

$$\mathrm{i}\hbar\frac{\partial\Psi}{\partial t}=\left\{\sum_{k=1}^{2}\left[-\frac{\hbar^2}{2\mu_k}\frac{\partial^2}{\partial r_k^2}+\frac{1}{2\mu_k r_k^2}\times\left(p_{\theta_k}^2+\frac{1}{\sin^2\theta_k}p_{\phi_k}^2\right)\right]+V(r_1,r_2;t)\right\}\Psi, \quad (14)$$

where the time-dependence of the potential comes from the time-dependence of the classical variables, we obtain the following set of differential equations for the center of the trajectory $r_k(t)$, the momentum $p_k(t)$, the width $A_k(t)$ and the phase $\gamma_k(t)$:

$$\dot{r}_k(t)=p_k(t)/\mu_k, \quad (15)$$

$$\dot{p}_k(t)=-V'_{\mathrm{eff},k}, \quad (16)$$

$$\dot{A}_k(t)=-\frac{2}{\mu_k}A_k(t)^2-\frac{1}{2}V''_{\mathrm{eff},k}, \quad (17)$$

$$\dot{\gamma}_k(t)=\frac{p_k(t)^2}{\mu_k}-\mathrm{i}\hbar\frac{\mathrm{Im}A_k(t)}{\mu_k}, \quad (18)$$

where $V'_{\mathrm{eff},k}$ and $V''_{\mathrm{eff},k}$ are effective forces which can be derived on general grounds by using the Dirac–Frenkel variational principle [1,3,4]. However, since the solution of the problem is independent of the forces (only the convergence pattern is affected) we can choose to use the leading terms of these forces, which (see [3,4]) are the classical forces. Thus for the first derivative we use $V'_{\mathrm{eff},k}=(\partial/\partial r_k)V_{\mathrm{eff}}$, where

$$V_{\mathrm{eff}}=V(r_1,r_2,t)+\sum_{k=1}^{2}\frac{1}{2\mu_k r_k^2}\left(p_{\theta_k}^2+\frac{1}{\sin^2\theta_k}p_{\phi_k}^2\right) \quad (19)$$

and hence Eqs. (15) and (16) show that the center of the packet moves as a classical trajectory. If also

the second derivative is taken as $V''_{\mathrm{eff},k} = (\partial^2/\partial r_k^2)V_{\mathrm{eff}}$ not only the grid point positions vary with time, as mentioned before, but so do the grid spacings, being a function of $A_k(t)$. In some cases, as the one under investigation, the equations of motion can lead to large values of $\mathrm{Im}A_k(t)$ thus, to prevent the grid points from collapsing in a very narrow region, an approach where $\mathrm{Im}A_k(t)$ is constant can be convenient. This fixed-width treatment is achieved by putting

$$V''_{\mathrm{eff},k} = 4\mathrm{Im}A_k(t)^2/\mu_k \tag{20}$$

instead of the second derivative of the potential and $\mathrm{Re}A_k(t_0) = 0$. Fig. 1 shows the motion of the central grid point in $r_{\mathrm{H}_2}$ (corresponding to the classical behavior) and its neighbors as a function of time for a variable (panel a) and for a fixed width approach (panel b).

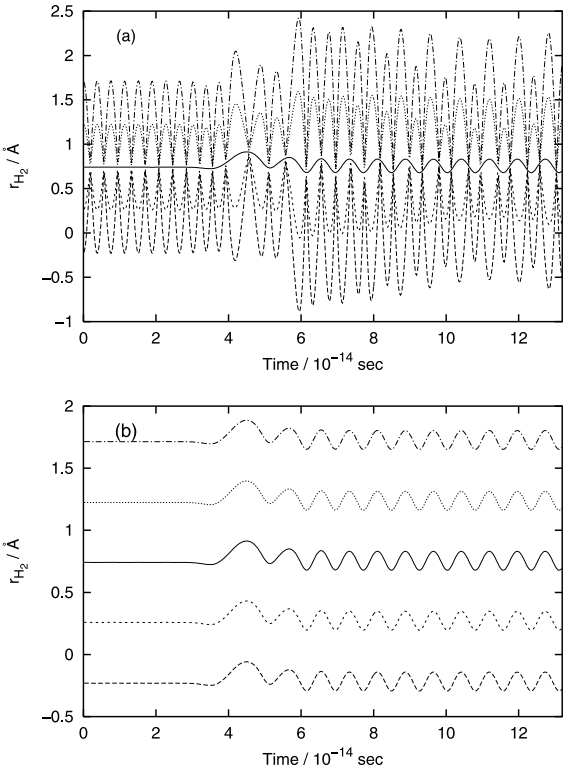


Fig. 1. Position of the grid points in $r_{\mathrm{H}_2}$ as a function of time. The solid line represents the behavior of the central grid point (the classical trajectory) which is identical in a variable width (panel a) and in a fixed width (panel b) approach. The other lines represent the neighbor grid points. It can be noticed how in this case a fixed width treatment is much more stable.

Together with Eqs. (15)–(18) the following set of differential equations for the expansion coefficient is obtained:

$$\mathrm{i}\hbar\dot{a}_{n_1n_2} = \sum_{m_1m_2} a_{m_1m_2} W_{n_1n_2;m_1m_2} + a_{m_1m_2}\Bigg[(2n_1+1) \times \frac{\hbar\mathrm{Im}A_1}{\mu_1} + (2n_2+1)\frac{\hbar\mathrm{Im}A_2}{\mu_2}\Bigg]\delta_{n_1m_1}\delta_{n_2m_2}, \tag{21}$$

where

$$W_{ij,i'j'} = \langle\phi_i\phi_j|V(r_{1i}, r_{2j}) - V'_{\mathrm{eff},1}(r_{1i} - r_1(t)) - V'_{\mathrm{eff},2}(r_{2j} - r_2(t)) + -\frac{1}{2}V''_{\mathrm{eff},1} \times (r_{1i} - r_1(t))^2 - \frac{1}{2}V''_{\mathrm{eff},2} \times (r_{2j} - r_2(t))^2|\phi_{i'}\phi'_j\rangle. \tag{22}$$

Now if we put

$$d_{ij} = c_{ij}\sqrt{\mathscr{N}_i^{(1)}\mathscr{N}_j^{(2)}} \tag{23}$$

into Eq. (21) together with Eq. (4) we get

$$\mathrm{i}\hbar\dot{d}_{ij} = W_{ij;i'j'}d_{ij}\delta_{ii'}\delta_{jj'} + \frac{\hbar\mathrm{Im}A_1}{\mu_1}\sum_{k=1}^{N_1} d_{kj}T_{ik}^{(1)}\delta_{jj'} + \frac{\hbar\mathrm{Im}A_2}{\mu_2}\sum_{k=1}^{N_2} d_{ik}T_{jk}^{(2)}\delta_{ii'}, \tag{24}$$

where

$$T_{ik}^{(1)} = \frac{1}{\sqrt{\mathscr{N}_i^{(1)}\mathscr{N}_k^{(1)}}}\sum_{n_1=0}^{N_1-1}\phi_{n_1}(z_i)(2n_1+1)\phi_{n_1}(z_k) \tag{25}$$

$$T_{kj}^{(2)} = \frac{1}{\sqrt{\mathscr{N}_j^{(2)}\mathscr{N}_k^{(2)}}}\sum_{n_2=0}^{N_2-1}\phi_{n_2}(z_j)(2n_2+1)\phi_{n_2}(z_k). \tag{26}$$

Thus the potential matrix is diagonal and the kinetic energy terms are block diagonal, so that the matrix coupling the grid points is sparse, which makes it particularly convenient using the Lanczos method to propagate Eq. (24).

## 3. Initialization and analysis

The initialization of classical variables has been carried out as in [12], that is starting with random values, while the initial distance $r_3$ was taken sufficiently large in order for the interaction potential to become negligible.

Concerning the initialization of the quantum wave packet the initial wave function is taken as the product of two Morse oscillator wave functions representing the vibrations of the two molecules

$$\psi(r_1, r_2, t=0) = \Psi_{v_1}^{\text{Morse}}(r_1)\Psi_{v_2}^{\text{Morse}}(r_2) \tag{27}$$

so that to have the initial expansion coefficients $d_{ij}(t_0)$ we need to project the initial wave function (27) onto the G-H functions

$$\begin{aligned} d_{ij}(t_0) = & \left(\frac{\hbar}{2\text{Im}A_1(t_0)}\right)^{1/4}\left(\frac{\hbar}{2\text{Im}A_2(t_0)}\right)^{1/4} \\ & \times \exp\left(\frac{\mathrm{i}}{\hbar}[p_{r_1}(t_0)(r_{1i}-r_1(t_0)) \right. \\ & \left. + \text{Re}A_1(t_0)(r_{1i}-r_1(t_0))^2]\right) \\ & \exp\left(\frac{\mathrm{i}}{\hbar}[p_{r_2}(t_0)(r_{2j}-r_2(t_0)) + \text{Re}A_2(t_0)(r_{2j} \right. \\ & \left. - r_2(t_0))^2]\right)\frac{1}{\sqrt{\mathcal{N}_i^{(1)}\mathcal{N}_j^{(2)}}}\Psi_{v_1}^{\text{Morse}}(r_{1i})\Psi_{v_2}^{\text{Morse}}(r_{2j}). \end{aligned} \tag{28}$$

The dynamical evolution of the system in time is thus studied by simultaneously propagating the equations of motion for classical variables integrated together with the set of Eqs. (15)–(18) and the differential Eq. (24) for the $d_{ij}$'s. In practice for each time-step $\Delta t$ the equations for the classical variables plus Eqs. (15)–(18) have been propagated with a predictor–corrector method, while for Eq. (24) a Lanczos procedure has been used. The accuracy of the integration procedure can be verified by checking the conservation of the norm of the wave function, of total energy and of total angular momentum.

Every trajectory obtained in the dynamical propagation of the system can either be nonreactive, reactive or, unlike pure classical trajectory methods, only part of the wave packet can react. Thus we can obtain information on probabilities for the reactive event or for inelastic scattering. As a matter of fact, as shown in [8,9], $|d_{ij}|^2$ represents the probability for being at the grid point $i$ in $r_1$ and $j$ in $r_2$. In order to have the reaction probability $P(t)$ then, it is sufficient to sum over those grid points in correspondence of which $r_2 \geqslant r_2^*$, that is where the CN bond can be considered as broken:

$$P(t) = \sum_i \sum_{j \geqslant j^*} |d_{ij}(t)|^2. \tag{29}$$

Within this approach it is not necessarily to insert an absorbing potential as we did in [12], provided that a sufficient number of grid points to follow the dynamics is employed (see the following).

Note that, as the grid moves, the grid point $j^*$ corresponding to $r_2^*$ is not fixed, but moves in time. As for a mixed quantum classical method, for each trajectory the probability $P(t)$ is not necessary an integer, as it happens in classical mechanics where the only two possibilities are that of a nonreactive event ($P(t) = 0$) or of a completely reactive collision ($P(t) = 1$).

In Fig. 2 we reported the probability amplitude $|d_{ij}|^2$ at different propagation times for a trajectory leading to a noninteger reaction probability: the wave packet splits, partly remaining on the nonreactive part of the grid, while the rest moves to the region where $r_2 \geqslant r_2^*$.

In a sense $d_{ij}$ also gives a measure of how much the system behaves in a quantum manner: if the system was completely classical we would have $d_{ij} = 1$ for the central point of the grid, which moves according to the classical equations of motion (15) and (16), while for the other DVR points $d_{ij}$ would be zero. As the behavior of the system differs from a pure classical description, their value increases, starting from the points placed closer to the classical trajectory. This situation is illustrated in Fig. 3 where the behavior of the $d_{ij}$'s for the central grid point and its neighbors is shown. For simplicity we have reported a situation where only 15 points in $r_{H_2}$ and 11 points in $r_{CN}$ have been employed. Panel (a), where $\sum_i |d_{ij}|^2$ is reported as a function of time, illustrates the behavior of $r_{H_2}$. It can be seen how the central

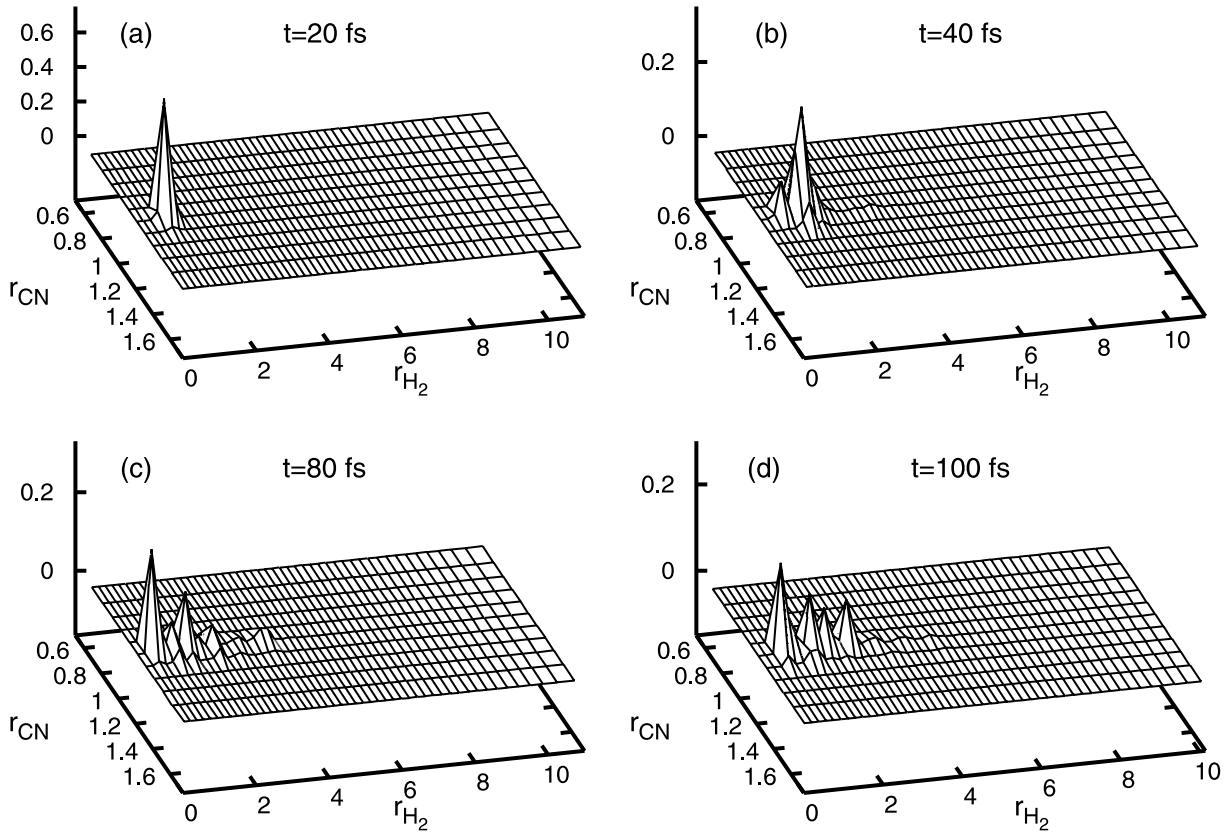


Fig. 2. Probability amplitude $|d_{ij}|^2$ at different propagation times. At the beginning of time propagation the largest amplitude is located in the nonreactive region of the grid, but as the time elapses it spreads, moving to the the region of large $r_{H_2}$. However, part of the wave packet, following the classical trajectory, remains on the nonreactive area.

point, i.e., the classical trajectory, shows the largest value and a regular pattern at the beginning of time propagation, due to the pure vibration of the diatom. When the interaction with CN becomes important the value of $\sum_i |d_{ij}|^2$ for this point suddenly decreases, while its neighbors show an increasing population, until the behavior becomes chaotic.

Panel (b) shows $\sum_j |d_{ij}|^2$, that is the $r_{CN}$ behavior, as a function of time. Here we can already notice that only few grid points in this degree of freedom are necessary to accurately describe the CN vibration. Only the central point shows a significant population before the collision: its value is nearly unity before the collisional event, and afterwards it decreases a little and shows a regular pattern, due to vibrational excitation, thus confirming that the bond is rather stiff and acts essentially as a spectator for the reaction.

Initially state selected cross-sections have been obtained from the reaction probability (Eq. (29)) by the expression [15]:

$$\sigma_{v_1,v_2,j_1,j_2} = 2\pi \int_0^{b_{\max}} P^R_{v_1,v_2,j_1,j_2} b \, \mathrm{d}b, \tag{30}$$

where $b$ is the impact parameter, $v_1$, $v_2$, $j_1$ and $j_2$ are the initial vibrational and rotational quantum numbers of the diatoms, respectively. We notice that the initialization of the rotational degrees of freedom is done in the same manner as in quasi-classical trajectory methods. This is a consequence of placing just one grid point (the classical limit) in these degrees of freedom.

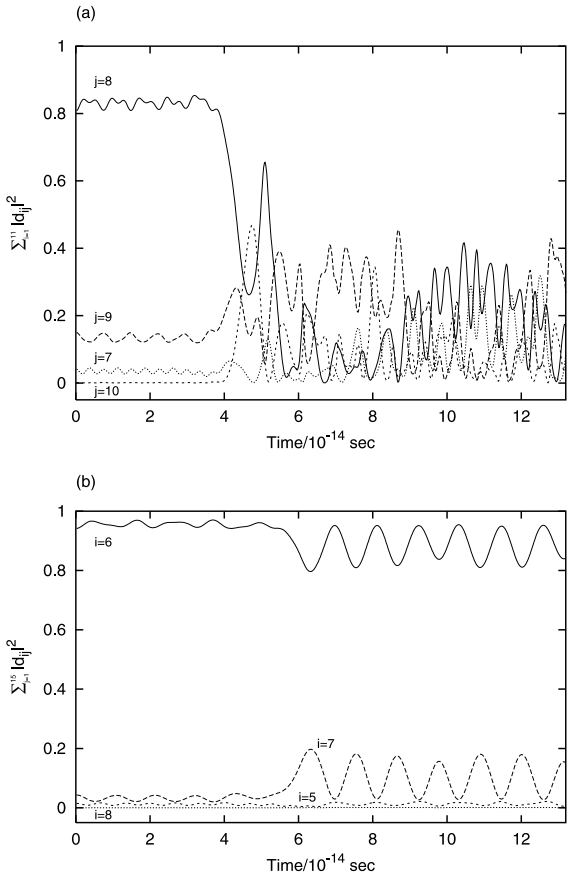


Fig. 3. $\sum_i |d_{ij}|^2$ (panel a) and $\sum_j |d_{ij}|^2$ (panel b) as a function of time for a grid of 11 points in $r_{CN}$ and 15 points in $r_{H_2}$ for the same trajectory of Fig. 2. In both cases the solid line is the central grid point in that specific degree of freedom, while the other lines stand for the neighbor points. The behavior of $r_{H_2}$ shows a strong quantum character, especially after the collision with CN: the value of $\sum_i |d_{ij}|^2$ for the central point ($j = 8$) presents a dramatic decrease whereas the other points acquire larger values. Concerning the behavior of $r_{CN}$ (panel b) only after the collision the grid point closest to the classical trajectory is sensibly different from zero due to the gained vibrational excitation, while all the other points have nearly a zero population. Only few grid points in this degree of freedom are thus needed for an accurate description.

Thermal rate constants can also be obtained as illustrated in [12], however, since the aim of this work is an exploration of the possibility of employing the time-dependent DVR method in the calculation of dynamical quantities for many body reactive problems, only initially state selected cross-sections for the vibrational ground states of the reagents have been calculated.

## 4. Results and discussion

The calculation of initially state selected cross-sections was carried out by running 2500 trajectories at each value of the energy, the integration was performed with a time-step $\Delta t = 0.2$ fs and using a value $r_2^* = 2.2$ Å for the calculation of reaction probabilities.

Trajectories were terminated either when the value of the distance between the two centers of mass $r_3$ was larger than 8 Å, or when $r_2 > 7$ Å or when the propagation time was over 7 ps. A crucial point in the calculation is the number of Hermite polynomials to be used in the G-H expansion (Fig. 4). For the CN bond we found that 11 DVR-points were sufficient for an accurate description, in agreement with the considerations drawn in the previous section (Fig. 3b).

The situation is different for $H_2$: Fig. 4 shows the reaction probability for a trajectory calculated with different numbers of DVR grid points in $r_{H_2}$. Convergence is generally obtained by using about 200/250 points. However this is the case only when the wave packet splits: the center of the wave packet follows the classical trajectory, oscillating around the equilibrium bond distance, while the most energetic parts of the packet move rapidly in the direction of large $r_{H_2}$, so a large number of grid points is needed in order to follow their dynamics. When we have a classical-like behavior (totally reactive or nonreactive) much less points are necessary, because the evolution of the system occurs locally and it is followed by the dynamics of the central point of the grid.

Since an increase of the number of DVR points corresponds to a strong increase of the computational time needed (the bottle neck being the Lanczos propagation) calculations were performed employing 81 Hermite polynomials in $r_{H_2}$ for classically behaving trajectories (which are the majority) while for wave packets spreading on the whole grid 241 DVR points were used.

Note that another way of circumventing the problem is to split the wave packet by re-expanding

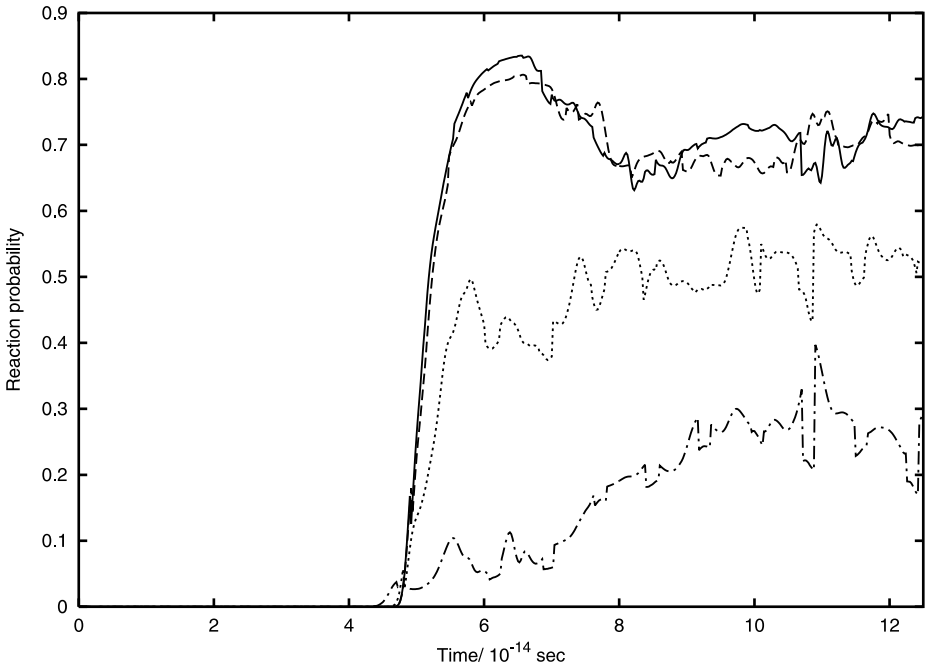


Fig. 4. Reaction probability for the same trajectory is shown in Fig. 3, but calculated with different numbers of grid points in $r_{H_2}$. The solid line is the reaction probability as a function of time using 251 grid points in $r_{H_2}$, the dotted line was calculated with 201 points, the dashed line with 151 points and the dashed-dotted line with 81 points.

the wave function in two DVR basis sets and following each of them separately, thus reducing the numerical effort. In addition this has another advantage: when the number of DVR points is increased, since they are equally distributed at larger and smaller values with respect to the center of the classical trajectory, part of them lies in the region where $r_{H_2} \approx 0$, where the amplitude $d_{ij}$ is obviously zero, so their inclusion does not lead to any gain in the dynamical description. In this way the numerical effort associated to the increased number of points does not correspond to an equally increased accuracy in the evaluation of reaction probability. This is partially avoided splitting the wave packet because the number of points is increased locally, i.e., only where they are needed.

From the computational point of view this method as described here is more time consuming than the grid method applied in [12] for the same system; anyway if we apply the combined Lanczos-split method introduced in [11] the number of Lanczos iterations requested for the time propagation is drastically reduced, the computational time decreases by a factor 2, thus becoming very competitive.

In Fig. 5 we have reported initially state selected cross-sections as a function of the initial translational energy for both the reactants in their ground states. Comparison is shown with 6D quantum dynamical calculations [16], a quasi-classical study [13] and our mixed quantum-classical method of [12].

Our calculation lies between quasi-classical and quantum results, approaching the first at low energy values and the latter as the energy increases. This can be easily explained noticing that whenever the wave packet splits the classical trajectory remains on the nonreactive side of the moving grid: this type of trajectories in a pure classical approach would not contribute to the reaction probability. Quantitatively the number of these trajectories increases with the energy, for instance we found that at 1500 $cm^{-1}$ they amount to less

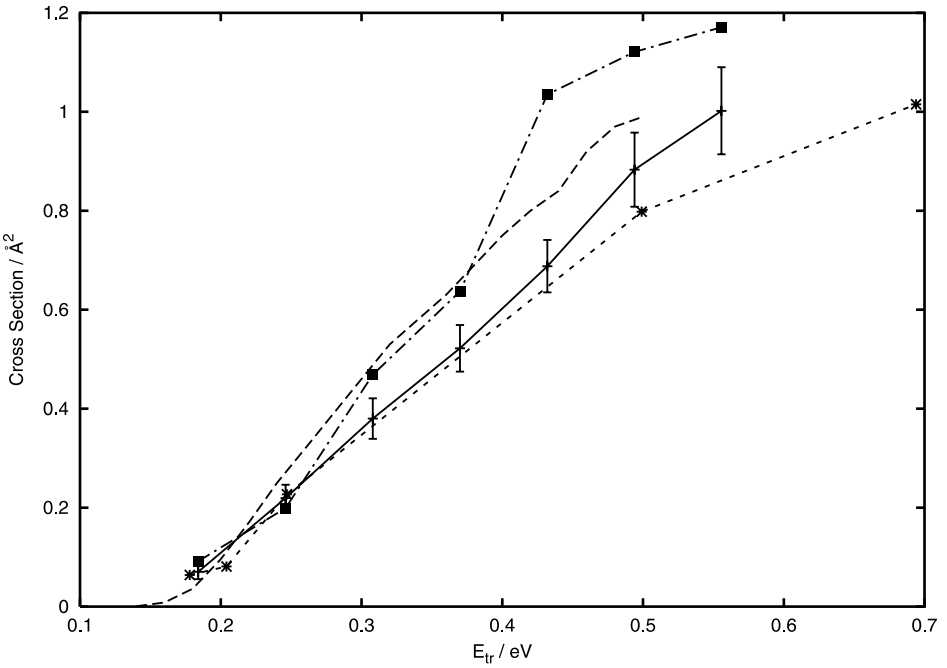


Fig. 5. Initial state selected cross-sections (Eq. (30)) as a function of initial translational energy for reagents in their ground states (solid line). Results from 6D quantum calculations [16] (dashed line), the quasi-classical trajectory study of [13] (dotted line) and our mixed quantum-classical method of [12] (filled squares) are also shown for comparison. The accuracy of our results has been evaluated by [17] $\Delta P_i^R = (N_i/N_{\rm tot})(N_i^{-1} - N_{\rm tot}^{-1})^{1/2}$, where $N_i$ is the number of reactive trajectories ($N_i$ is not necessary an integer as in classical dynamics).

than 0.5% of the total trajectories, while at 4500 cm$^{-1}$ they are about 3.5% and their contribution becomes significant.

The agreement with the quantum behavior of [16] can obviously be improved by including other degrees of freedom in our quantum treatment, however part of the discrepancy, above all at high energies, can also be due to the possibility that some parts of the wave function which move very fast cannot be appropriately followed by the grid, thus leading to a slight underestimation of the reaction probability (of course this can be avoided increasing the number of grid points at high energy in order to cover that region).

Concerning comparison with the mixed quantum-classical method we used in [12], there we also found a behavior generally lying between the classical and 6D quantum results (also for cross-sections of excited initial vibrational levels), but the pattern was not so regular as in the method employed here, as it can be seen from Fig. 5. This is due on one hand to the more significant sample used here (2500 trajectories instead of 1500), but another reason is that that method is a primitive quantum-classical model, partly neglecting quantum-classical correlation, whereas the time-dependent DVR method is rigorously derived from first principles (for a discussion see for example [5]).

In conclusion, we have shown how the introduction of a quantal treatment of some of the degrees of freedom within the time-dependent DVR method [8] described in Section 2 leads to results which are satisfying both from a computational point of view and from a comparison with quantum values. Indeed our results lie between classical and quantum calculations, approaching the latter for large values of the energy, that is where the discrepancy between the two treatments is more evident.

For this reason we expect that the treatment of all the degrees of freedom of the system with the

time-dependent DVR method will lead to excellent results. That our previous semi-classical results is in slightly better agreement with the 6D quantum results than the present, could be due to the use of an effective potential for the classical degrees of freedom. We have previously noticed that part of the so-called quantum-classical correlation [1] can be accounted for by using an effective potential. However, the present TDGH-DVR method is the rigorous answer to the question: given that the system degrees of freedom are treated by classical mechanics – what is the systematic way of improving this description – so as to approach the full quantum mechanical limit. This does not rule out that other descriptions derived on less rigorous grounds can occasionally give slightly better agreement with more exact numbers.

## Acknowledgements

This research is supported by the EU-TMR grant: HPRN-CT-1999-00005 and the Carlsberg Science Foundation.

## References

[1] G.D. Billing, J. Chem. Phys. 107 (1997) 4286.
[2] G.D. Billing, Mixed quantum-classical methods, in: H.F. Schaefer III (Ed.), Encyclopedia of Computational Chemistry, Wiley, New York, 1998.
[3] G.D. Billing, J. Chem. Phys. 110 (1999) 5526.
[4] G.D. Billing, Chem. Phys. 242 (1999) 341.
[5] G.D. Billing, Quantum-classical methods, in: A. Lagan'a, A. Riganelli (Eds.), Lecture Notes in Chemistry: Reaction and Molecular Dynamics, Springer, Berlin, 2000.
[6] G.D. Billing, S. Adhikari, Chem. Phys. Lett. 309 (1999) 249.
[7] S. Adhikari, G.D. Billing, J. Chem. Phys. 113 (2000) 1409.
[8] S. Adhikari, G.D. Billing, Chem. Phys. Lett. 321 (2000) 197.
[9] G.D. Billing, Chem. Phys. 264 (2001) 71.
[10] G.D. Billing, J. Chem. Phys. 114 (2001) 6641.
[11] G.D. Billing, Chem. Phys. Lett. 339 (2001) 237.
[12] C. Coletti, G.D. Billing, J. Chem. Phys. 113 (2000) 11101.
[13] M.A. ter Horst, G.C. Schatz, L.B. Harding, J. Chem. Phys. 105 (1996) 558.
[14] G.D. Billing, J. Phys. Chem. 105 (2001) 2340.
[15] N. Balakrishnan, G.D. Billing, J. Chem. Phys. 101 (1994) 2785.
[16] W. Zhu, J.Z.H. Zhang, Y.C. Zhang, Y.B. Zhang, L.X. Zhan, S.L. Zhang, D.H. Zhang, J. Chem. Phys. 108 (1998) 3509.
[17] H. Essen, G.D. Billing, M. Baer, Chem. Phys. 17 (1976) 443.